Cavitation of Langmuir monolayers

Z. Khattari,[1] E. Hatta,[1] P. Heinig,[1] P. Steffen,[1] Th. M. Fischer,[1,*] and R. Bruinsma[2,3]
[1]*Max Planck Institute of Colloids and Interfaces, Am Mühlenberg 1, 14476 Golm, Germany*
[2]*Physics Department, University of California, Los Angeles, California 90024*
[3]*Instituut-Lorentz voor Theoretische Natuurkunde, Universiteit Leiden, Postbus 9506, 2300 RA Leiden, The Netherlands*
(Received 17 October 2001; published 2 April 2002)

Cavitation in liquid expanded and liquid condensed Langmuir monolayers induced by laser heating or microbubble coalescence is studied experimentally using fluorescence and Brewster angle microscopy. The kinetics of hole closure of two-dimensional (2D) gaseous cavitation bubbles exhibits a decelerated dynamics for cavities surrounded by a liquid expanded phase and an accelerated dynamics for cavities in a liquid condensed phase. Most of the cavities in liquid condensed phases possess a nonconvex shape and do not close. The results are compared with theoretical predictions derived for 2D cavitation of liquid monolayers of different surface shear viscosities, and for solid monolayers with diffusive flux of vacancies and interstitials. While part of the theory is in qualitative agreement with the experiment, the experimentally observed hole persistence within the liquid condensed phases and the hole closure within liquid expanded phases remains to be explained. The technique of microbubble coalescence might be particularly useful for the study of the rheological properties of hexatic phases.

DOI: 10.1103/PhysRevE.65.041603 PACS number(s): 68.47.Pe, 47.55.Bx, 83.80.Qr

I. INTRODUCTION

The properties of a material undergo a dramatic change at the melting transition. In the solid phase, materials maintain—more or less indefinitely—their shape while a liquid adopts the shape of its container. In more precise language, a solid responds to shear stress by elastic deformation, characterized by a shear modulus, while a liquid responds to shear stress by hydrodynamic flow, characterized by a shear viscosity.

The difference between these two forms of behavior is illustrated in an appealing manner by the phenomenon of *cavitation*. Cavities in liquids are generated, for instance, by intense sound waves or by the action of ship propellers. In a classical paper [1], Lord Rayleigh showed that the lifetime τ of a spherical cavity inside a three-dimensional (3D) inviscid fluid is proportional to the (initial) cavity radius a: $\tau(a) = 0.915a(\rho/\Delta P)^{1/2}$ with ρ the density of the fluid and ΔP the pressure difference between the cavity interior and the exterior surface of the fluid. For very viscous 3D fluids, τ is of order $\eta/\Delta P$ independent of the cavity radius (η is the shear viscosity).

Cavities in solids can be produced, for instance, by bombardment with a beam of noble gas atoms. These cavities shrink slowly and eventually disappear but the transport mechanism is not collective hydrodynamic flow but instead incoherent radial diffusion of vacancies and/or interstitials. An important distinction between cavities in fluids and in solids is the fact that a hollow cavity in a defect-free single crystal is not spherical. If the surface free energy is minimized at fixed cavity volume one obtains a convex faceted shape for the cavity that reflects the symmetry of the crystal (the cavity shape is obtained by the so-called Wulff plot [2]). If the cavity is sufficiently far from thermodynamic equilibrium, then concave cavity shapes can be encountered as well. Examples are dendrite formation during rapid crystallization and fracture patterns produced by the application of a large local stress on a solid.

These distinctions between the solid and liquid phases become somewhat more delicate for two-dimensional materials. It follows from fundamental statistical-mechanics arguments that 2D materials may be in a hexatic phase [3]. Hexatic materials have properties that in some sense are intermediate between those of the solid and liquid phases. Hexatics are characterized, for instance, by short-range positional order—as is true for liquids—but on the other hand they do have crystallographic directions with quasi-long-range order (''bond-orientational'' order). In terms of their response to shear stress, hexatics contain a finite concentration of free dislocations so their shear modulus is zero and they are able to flow. This means that shear flow is permitted, so cavities inside hexatics are expected to shrink and disappear by hydrodynamic flow. However, cavities in ordinary 2D isotropic liquids should have a circular shape but if the Wulff construction is applied to a finite-sized cavity in a hexatic, then a sixfold symmetric shape is obtained, resembling a hexagon with rounded corners.

There is currently considerable interest in the question of whether or not hexatic phases are present in the phase diagram of 2D Langmuir monolayers (LM's). LM's are monolayers of insoluble surfactants residing at the air-water interface. The pressure-temperature phase diagram of LM's exhibits a 2D isotropic gas (G) phase as well as a number of solid phases. The various liquid phases of LM's are divided into the ''liquid expanded'' (LE) and the ''liquid condensed'' (LC) phases. There is no doubt that the LE phase is just an isotropic 2D liquid. The nature of the LC phases is, on the other hand, more controversial. Evidence obtained from the line-shape analysis of grazing incidence x-ray diffraction [4–6] suggests that some of the LC phases are hexatics or tilted hexatics (in a tilted hexatic there is a preferred in-plane

*Email address: thomas.fischer@mpikg-golm.mpg.de

direction; for LM's this direction would be the average projection of the tails of the surfactant molecules in the plane of the air-water interface). The shape and texture of the LC-LE coexistence domains of these phases, as examined by polarized fluorescence, support this interpretation. However, the interpretation of the x-ray data has been questioned and it was suggested that these phases in reality might be highly defected solids [7,8].

Information concerning the response to shear stress of the putative hexatic LC phases would provide important evidence that could help to decide the issue. Macroscopic rheology experiments report that these phases indeed are fluid but with a shear viscosity that is strongly dependent on shear rate [9]. The interpretation of macroscopic rheology experiments is complicated, however, by the fact that it is not easy to distinguish a highly defected solid from a fluid with ''non-Newtonian'' flow properties. What is necessary are so-called microrheological studies carried out at sufficiently short length scales so that quenched-in defects cannot materially affect the results.

It is the aim of this paper to show that microcavitation experiments on LM's are practical and that observations on the formation and collapse of microcavities may provide a useful diagnostic tool for the identification of LM phases. In Sec. II, we first discuss experiments concerning the collapse of micrometer-sized cavities for three different types of surfactant, involving both the LC and LE phases. We then show the results of a study of the formation of cavities, produced by the application of a large but highly localized stress (''explosive cavitation''). In Sec. III we develop a simple theoretical description of cavitation formation and collapse in LM's. Section IV concludes with a comparison between theory and experiment.

II. EXPERIMENT

A. Materials and methods

Experiments on LM cavitation were performed using pentadecanoic acid (Sigma Aldrich), 10,12-pentacosadiynoic acid (Wako Pure Chemical Industries Ltd.) and octadecanol (Sigma Aldrich). The amphiphiles were chosen since either their phase diagram is known in detail (pentadecanoic acid and octadecanol) or their mechanical and rheological properties can be adjusted by photopolymerization (pentacosadiyonic acid). The LM was visualized either by fluorescence microscopy (FM) or by Brewster angle microscopy (BAM) using an Ar^+ laser in both cases. For the FM, 1% of fluorescence probe 4-hexadecylamino-7-nitrobenz-2-oxa-1,3-diazole was added to the surfactants. The LM also was exposed to a neodymium-doped yttrium aluminum garnet (Nd/YAG) ir laser with focus on the water-air surface (for FM, the same objective was used while, a second 20× objective was added for BAM with the focus arranged so that it coincided with the field of view of the Brewster angle microscope). The power P of the ir laser (after the objective) was adjustable in a range between 50 mW and 4 W. The ir laser locally heats the subphase producing a small hot spot. The temperature increase ΔT at the center of the hot spot is proportional to the laser power ($\Delta T = \alpha P$ with $\alpha = 10$ K/W).

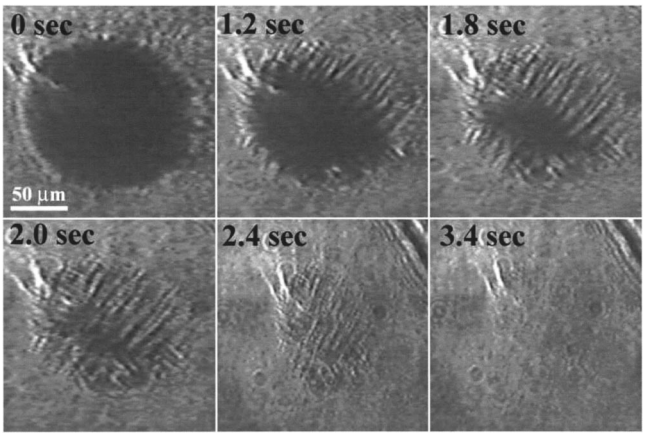

FIG. 1. Closure of a cavity in the LC phase of 10,12-pentacosadiynoic acid produced by low heating and observed with BAM. After the laser heating switch-off at $t=0$, dendritic growths are observed at the cavity surface. The dendrite structure disappears after cavity closure (final image).

The device has been described in more detail elsewhere [10]. Pentadecanoic acid and octadecanol (10,12-pentacosadiynoic acid) were spread from chloroform (benzene) without further purification. Exposure of the pentacosadiynoic acid monolayer to uv using a standard mercury lamp polymerizes the monolayer. Experiments were carried out with the monomer as well as with a polymerized monolayer.

B. Cavity collapse in the LC phase

Figure 1 shows BAM images of the LC phase of 10,12-pentacosadiynoic acid monomer at $\Pi = 25$ mN/m and $T = 18\,^{\circ}$C subjected to local ir laser heating with $P = 1.01$ W. The circular region in the laser focus has a reduced reflectivity, approximately comparable with that of the 2D G (gas) phase of 10,12-pentacosadiynoic acid.

After turning the laser off at $t=0$, the hole closed completely by inward growth of dendrites, developing from the cavity boundary. After cavity closure, the dendrite structure disappeared. We performed 210 closure experiments. Complete closure of the cavities was observed in 63 of the experiments (≈30%). In 147 of the experiments (≈70%), the cavities did not close completely, with the final radius roughly half the initial radius. Figure 2 shows the time dependence $a(t)$ of the radius of a number of cavities that did close completely. The cavity radius is plotted on a log-log scale as a function of $t_c - t$, with t_c the closure time [i.e., $a(t_c)=0$]. If the data are fitted with a power law

$$a \propto (t_c - t)^{\beta} \tag{1}$$

we obtain exponents β in the range 0.2 ± 0.1. A distribution of the exponent is plotted in the inset of Fig. 2. It is obtained from the evaluation of 30 randomly chosen complete closure events.

If one polymerizes the pentacosadiynoic acid it is no longer possible to form a hole in the monolayer using laser heating, so that no hole closure events exist for the polymer.

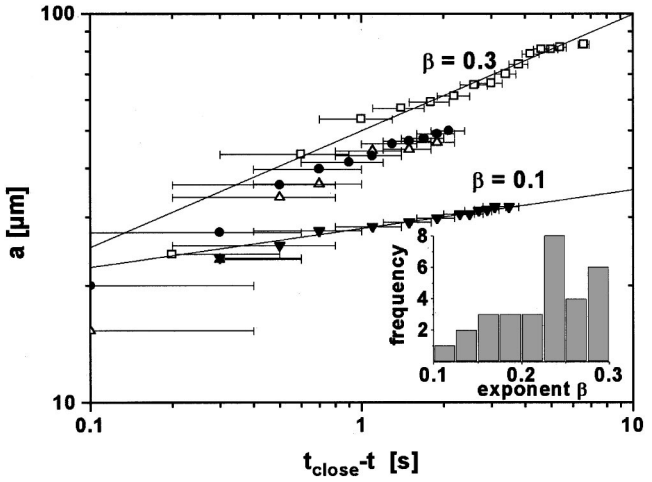

FIG. 2. Cavity closure kinetics of four cavities in the LC phase of 10,12-pentacosadiynoic acid (with complete closure). The solid lines represent power law fits with exponents $\beta = 0.1-0.3$. A distribution of exponents from 30 randomly chosen complete closure events is added in the inset.

C. Cavity collapse in the LE phase

For purposes of comparison, we next studied cavity collapse in the (isotropic liquid) LE phase. Figure 3 shows successive FM images of the closure of a cavity in the LE phase of pentadecanoic acid ($A = 76.5$ Å^2, $T = 22\,^\circ$C).

Cavities formed again at the focus of the ir laser (dark regions in Fig. 3). The higher heating levels in this case produced convective hydrodynamic flow in the subphase. This convection produced at the surface leads to a flow of the LM, roughly along a radial inward direction toward the laser focus. Because the flow was not radially symmetric, the cavity (or cavities) were translated and deformed by the flow, producing the ''footprint shape'' visible in Fig. 3. We performed 18 closure experiments. After the heating was switched off, the cavities all closed completely. The motion of the footprint cavity after switch-off, visible in Fig. 3, is

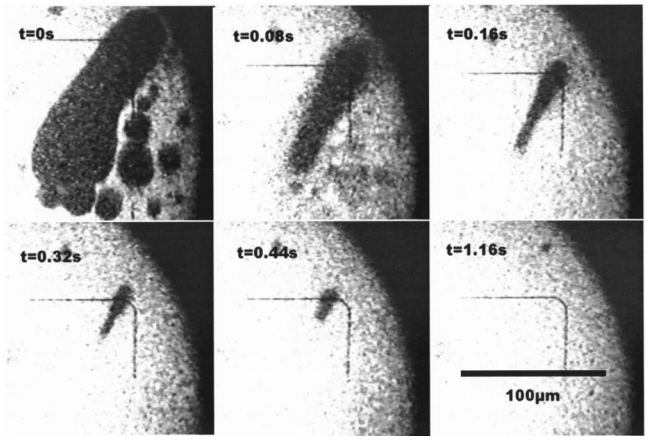

FIG. 3. Closure of cavities in the LE phase of pentadecanoic acid ($A = 76.5$ Å^2, $T = 22\,^\circ$C). During heating ($t < 0$), hydrodynamic flow distorted the largest of the bubbles, producing a ''footprint'' shape. After switching the ir heating off at $t = 0$, all cavities closed completely.

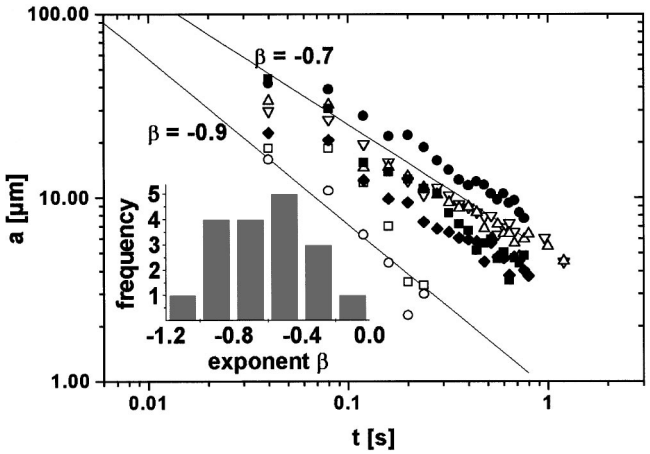

FIG. 4. Cavity closure kinetics in the LE phase of pentadecanoic acid. The cavities closed according to a power law, with negative exponents $\beta = -0.8 \pm 0.1$. A distribution of exponents from 18 randomly chosen closure events is added in the inset.

due to decaying residual hydrodynamic flow.

We plotted the equivalent radius of the footprint cavity defined by

$$a = \sqrt{A/\pi} \tag{2}$$

as a function of time in Fig. 4 (A is the area of the cavity). The data were again fitted with a power law (Fig. 4):

$$a \propto t^{\beta} \tag{3}$$

but we now obtain a *negative* exponent β in the range -0.8 ± 0.1. Note that this fitting form cannot hold for small t. A distribution of exponents from the individual closure events is plotted in the inset of Fig. 4.

D. Explosive cavitation

A different mode of cavity generation is encountered at increased power levels of the ir laser ($P > 1$ W). In that case, 3D micrometer-sized gas bubbles nucleate in the aqueous subphase below the LM due to the decrease of the solubility of gases in water with increasing temperature (see Fig. 5, first frame). Because the nucleation of the bubbles takes place entirely in the subphase, we can assume that the air-water surface of the bubbles is free of surfactants (which are highly insoluble). The bubbles rose to the surface with a speed of the order of 100 μm/s (consistent with the law of Hadamard and Rybzinki [11]). Arrival of the bubbles at the LM was easily visible by BAM, as shown in Fig. 5 (second frame, bright spot).

After a residency time at the surface of the order of seconds, the bubble bursts (Fig. 5, third frame). The bursting process must have taken place on submillisecond time scales, as was determined using a fast camera (time resolution 1/240 s). The bursting event looked surprisingly like an *explosion* on micrometer-level length scales: it was accompanied by the emission of a capillary shock wave. The shock wave can be seen as the region of increased reflectivity in Fig. 5 (third frame; the increased reflectivity is due to the deviation of the

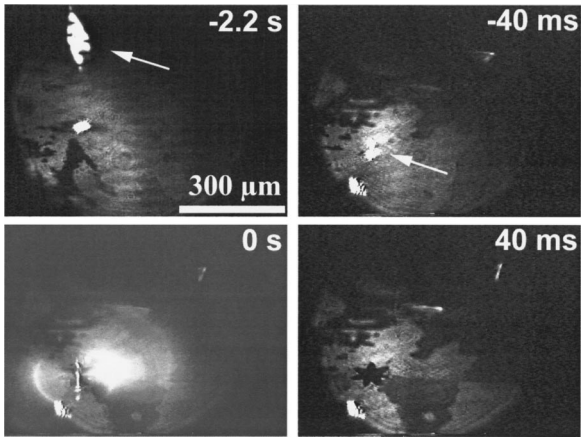

FIG. 5. BAM images of cavity formation by bubble bursting in an octadecanol LM ($T=25\,^{\circ}\mathrm{C}$, $\pi\approx 16.5$ mN/m). Heating by the ir laser caused nucleation in the subphase of a bubble of radius $R\approx 3\,\mu$m at time $t=-2.2$ s (white arrow, first frame). The bubble settled below the LM at $t=-40$ ms (second frame). Bubble bursting took place at $t=0$ (third frame), accompanied by capillary wave emission. After the rupture event, a star-shaped hole of radius $a\approx 10\,\mu$m was observed with concave surface sections (fourth frame).

angle between the incident Ar^{+} laser and the surface from the Brewster angle as well as between the local plane of incidence and the polarization vector of the laser). Relaxation of the capillary wave again took place on submillisecond time scales. After the capillary wave had disappeared, either a star-shaped or hexagonal hole emerged at the center of a reorganization zone (Fig. 5, fourth frame). Unlike the previous two cases, where cavities were produced by low-intensity heating, the holes persisted for hours without any evidence of area reduction.

Star-shaped cavities are observed predominantly for the case of small cavities while for larger cavities polygonal shapes most frequently with six facets are encountered. An example of the second case is shown in Fig. 6. In Fig. 7 we plot a distribution of the number of arms of the star-shaped holes and the number of edges of the polygonal holes, taken from 70 holes found in the monolayer.

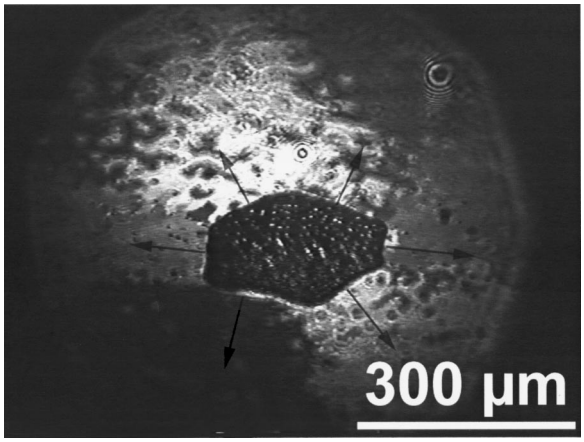

FIG. 6. BAM image of a hexagonal cavity in octadecanol ($T=25\,^{\circ}\mathrm{C}$, $\pi\approx 16.5$ mN/m) surrounded by a tilted L_2 phase. The cavity was produced by the bursting of a bubble. Gray arrows show the tilt direction of the LM as deduced from the gray scale of the image.

The LC phase in question (L_2) is tilted with a tilt direction toward the next nearest neighbors. The texture of the tilt director can be deduced from the BAM image and is shown in Fig. 6. Note the fact that the molecular tilt performs a 2π rotation as we traverse the cavity border. The vertices of the hexagonal boundary are the intersection points of the cavity surface with lines in the LM where the tilt direction undergoes a 60° rotation. Apparently, the micrometer-scale explosion has produced a *virtual topological defect* in the texture of the tilt director [12]. By a virtual defect we mean that if we mathematically extend the LM director pattern into the cavity, then a topological defect is produced, which is located inside the cavity.

The cavity interior is substantially darker than the surrounding area, suggesting that the interior is once again in the *G* phase. Moreover, surfactant—or insoluble, photochemical product—clusters produced by the explosion are visible inside the hole, and they exhibit pronounced Brownian motion. This indicates that the surface shear viscosity of the hole interior is low, supporting the conclusion that the cavity interior is in the *G* phase.

An interesting variant of the explosive cavitation scenario is shown in Fig. 8 for the case of 10,12-pentacosadiynoic acid: After the gas bubble came in contact with the LM, it produced a star-shaped hole. However, the bubble did not burst in this case, but apparently resealed. The bubble could be seen to move below the LM. After a time of order 0.1 s, it did burst, creating a second cavity. In contrast to the octodecanol case, no shock wave was observed in this case. Moreover the star shape eventually relaxed to a convex shape indicating shorter equilibration times for pentacosadiynoic acid. Nevertheless, as in the octodecanol case, the cavity never closed.

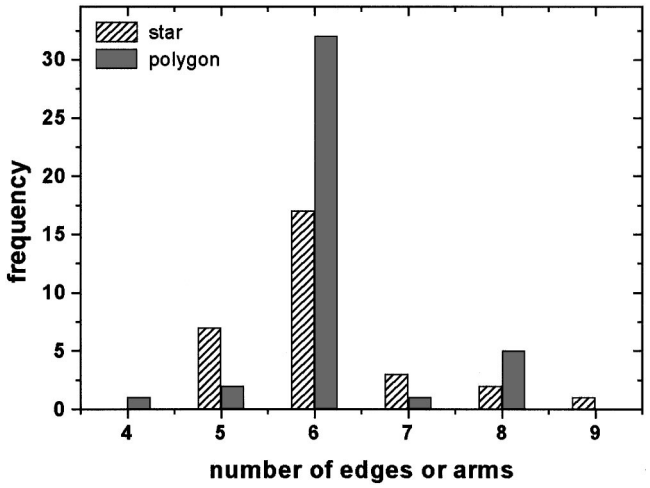

FIG. 7. Histogram of the shape of the holes created after bubble rupture taken from 70 different rupture events. Larger holes forming polygonal holes are more frequent than star-shaped holes, which form for smaller areas. Both distributions peak at a sixfold symmetric shape.

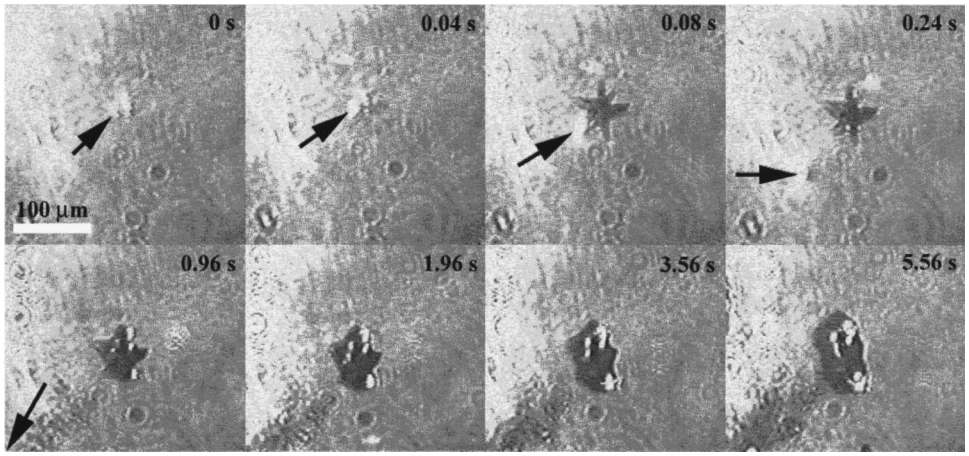

FIG. 8. BAM image of the formation of a star-shaped cavity in 10,12-pentacosadiynoic acid ($\pi = 25$ mN/m, $T = 18\,^{\circ}$C). A gas bubble (black arrow) creates a star-shaped cavity without bursting. The bubble continues to move below the LM, leaving behind a path of reduced density (darker). The star-shaped hole relaxes from a six-armed star (0.08 s) to a five-armed star (0.24–0.96 s), and then toward a convex-shaped cavity (0.96–5.56 s).

III. THEORY

In this section we use a combination of simple thermodynamic and hydrodynamic arguments to come up with a description of the formation and collapse of cavities in LM's allowing us to interpret the results obtained in Sec. II. We start with a discussion of the thermodynamics of cavities in LM's.

A. Inhomogenous LM's in mechanical equilibrium

In the experiments discussed in Sec. II, a small, circular patch of dilute gas phase, is produced inside a surrounding denser LC or LE film by steady-state local heating of the LM with a narrowly focused laser beam. The heat deposited by the beam is dissipated in the aqueous subphase, producing a radial symmetric temperature profile $T(r)$, with r the radial distance from the center of the cavity. It follows from the heat diffusion equation that $T(r)-T(\infty)\propto 1/r$ [with $T(\infty)$ the temperature far from the heated spot]. The thermodynamic environment of the LM is thus inhomogeneous. In addition, the LM cannot be in full thermodynamic equilibrium because a heat flux represents a source of entropy production. However, at sufficiently low heating levels the LM could still be in *mechanical equilibrium*. By this we mean that there are no unbalanced mechanical forces inside the LM and so there is no collective 2D mass transport (e.g., 2D hydrodynamic flow). Under these ''quasistatic'' conditions, which of course must be verified experimentally, the interior structure of the cavity can be inferred from the equilibrium phase diagram as follows.

In the absence of externally applied forces, the condition that there are no unbalanced mechanical forces inside a LM, is equivalent to stating that its surface tension γ is uniform (a nonuniform surface tension leads to mass transport). This does not mean, however, that the pressure Π of the LM is uniform. The local surface tension of a LM is the difference of the local temperature-dependent surface tension of pure water $\gamma_w(T)$ at the local temperature T and the local 2D surface pressure $\Pi(T)$ of the surfactants at that temperature, as determined by the equation of state of the LM. For a uniform surface tension, the quantity

$$\gamma_0 = \gamma_w(T) - \Pi(T) \tag{4}$$

must be constant. The value of the constant γ_0 is determined by evaluating Eq. (4) far from the cavity: γ_0 equals $\gamma_w(T_0)-\Pi(T_0)$, with $\gamma_w(T_0)$ the surface tension of water at the ambient temperature T_0 of the subphase, and with $\Pi(T_0)$ the pressure of the LM at the ambient temperature. Near the cavity, laser heating increases the temperature inversely proportionally to the distance r from the cavity. This reduces the surface tension $\gamma_w(T)$ of water below the asymptotic value $\gamma_w(T_0)$, approximately proportional to $T-T_0$. It then follows from Eq. (4) that the surface pressure of a locally heated LM is not uniform.

More precisely, if we traverse a path in the LM that starts inside the cavity and ends at the outer boundary of the LM, then we should traverse an *isotension line* in the Π-T phase diagram. Isotension lines are the loci of points in the Π-T plane with constant surface tension γ (approximately straight lines). In particular, we should traverse that isotension line which passes through the asymptotic temperature and pressure. In Fig. 9, we show an isotension line in a schematic phase diagram, with a single phase coexistence line.

We will assume that the temperature T_1 at the center of the disk $r=0$ is sufficiently high, so the disk center $r=0$ is in the G phase. The cavity boundary, located at $r=a$, is determined by the condition that $T(a)$ must be the intersection point of the phase boundary $\Pi_{ce}(T)$ with the isotension line (see Fig. 9). At time $t=0$, the laser beam is switched off. For a sufficiently narrow beam width, thermal diffusion will very rapidly establish isothermal conditions with $T=T_0$ everywhere. Inside the dense phase, the equilibrium pressure equals $\Pi(T_0)$ in thermodynamic equilibrium while inside the cavity the equilibrium pressure equals the coexistence pressure $\Pi_{ce}(T_0)$ at T_0 (see Fig. 9). The pressure difference $\Delta\Pi = \Pi(T_0) - \Pi_{ce}(T_0)$ represents a driving force for the collapse of the cavity.

B. Cavity collapse

1. Isotropic 2D fluids

During the collapse of the cavity, the work done by $\Delta\Pi$ must be balanced by viscous losses [13]. For an isotropic and fluid LM, there are two sources of viscous loss: energy dissipated by 2D flow of the surfactant molecules (flow velocity

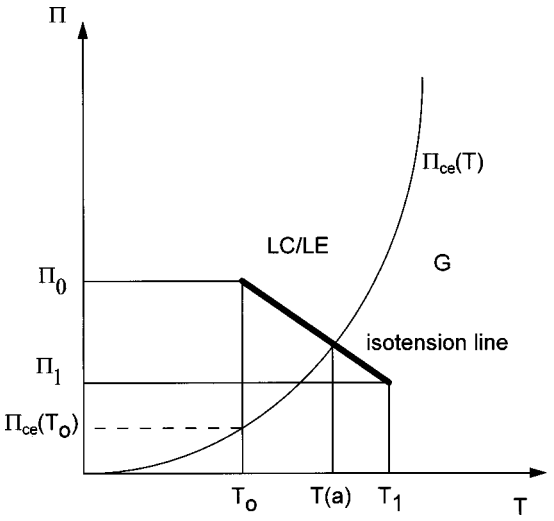

FIG. 9. Cavitation thermodynamics: isotension line is shown for cavitation in a schematic Π-T phase diagram with a single phase coexistence line $\Pi_{ce}(T)$. The pressure and temperature far from the cavity are, respectively, Π_0 and T_0. If an inhomogeneously heated LM is in mechanical equilibrium, then the set of allowed Π-T values is the isotension line that passes through Π_0 and T_0. At the center of the cavity, pressure and temperature are, respectively, Π_1 and T_1, while $T(a)$ is the temperature at the cavity surface. After laser switch-off, the temperature must equal T_0 everywhere.

$\vec{v}_2$) and energy dissipated by 3D subphase flow (flow velocity $\vec{v}_3$) entrained by the surface:

$$P(t)=\frac{1}{2}\eta_2\int d^2r(\partial_i v_{2j})(\partial_i v_{2j}) + \frac{1}{2}\eta_3\int d^3r(\partial_i v_{3j})(\partial_i v_{3j}) \quad (5)$$

with $\eta_{2,3}$ the surface (bulk) viscosities. The surface flow velocity can be obtained directly if the LM can be assumed to be incompressible. In that case, mass conservation requires that, for radial symmetry, the flow velocity is inversely proportional to r. Demanding that the flow velocity at $r=a$ equals the velocity da/dt of the cavity surface gives

$$v_2(r)=\frac{da}{dt}(a/r) \quad (r>a). \quad (6)$$

Radial surface flow inside the cavity would lead to accumulation of surfactant material at the cavity center $r=0$. Under steady-state conditions, this is not possible so we must assume that there is no surface flow inside the cavity:

$$v_2(r)=0 \quad (r<a). \quad (7)$$

More precisely, it can be shown that surface flow inside the cavity can be neglected for values of r less than $a-\delta$, where $\delta=\eta_3 D/E$ with D the diffusion constant and E the area modulus of the gas phase.

In order to obtain $\vec{v}_3$, we must solve the 3D Navier-Stokes equation in the limit of low Reynolds numbers:

$$\eta_3\Delta\vec{v}_3=-\vec{\nabla}P,$$

$$\vec{\nabla}\cdot\vec{v}_3=0. \quad (8)$$

The boundary conditions for the solution of Eq. (8) are (i) that at the LM surface ($n=0$) the normal component of $\vec{v}_3$ vanishes, and (ii) that for $n=0$ the in-plane component of $\vec{v}_3$ must equal $\vec{v}_2$, as given by Eqs. (6) and (7). The solution of Eq. (8) under the stated boundary conditions was obtained by de Koker and McConnell [14] in a different context:

$$v_n(r,n)/\dot{a}=-\int_0^\infty dk\, aJ_0(ka)(kn)J_0(kr)e^{-kn},$$

$$v_r(r,n)/\dot{a}=-\int_0^\infty dk\, aJ_0(ka)(1-kn)J_1(kr)e^{-kn} \quad (9)$$

with $J_{0,1}(x)$ Bessel functions.

We will obtain the rate law for the collapse of the cavity as follows. Note that there is a mathematical singularity in the flow field at the cavity border $r=a$. During the collapse of a cavity, the surface tension of the LM (and hence the pressure) is no longer uniform because of the presence of 2D and 3D viscous stress applied to the LM. Because $\Delta_\perp\vec{v}_2=\vec{0}$ for the radial flow pattern of Eq. (7), there is actually no contribution from the surface viscous force per unit area, which is equal to $\eta_2\Delta_\perp\vec{v}_2$. The force per unit area applied by the viscous stress tensor of the subphase on the LM thus must be balanced completely by the gradient of the surface tension:

$$\vec{\nabla}_\perp\gamma=\eta_3\frac{\partial}{\partial n}\vec{v}_3(r,n=0). \quad (10a)$$

To obtain the surface tension, Eq. (10a) must be integrated. The integration must be carried out keeping in mind that (i) the surface tension at infinity equals γ_0, (ii) the surface tension inside the cavity is close to that of water, and (iii) at the cavity boundary $r=a(t)$ the surface tension must undergo a discontinuous change $\delta\gamma(a)$ given by

$$\delta\gamma(a)=-2\eta_2\dot{a}/a. \quad (10b)$$

Equation (10b) is a consequence of the fact that the *total* surface stress tensor, i.e., the sum of the surface viscous stress and the surface tension, must be continuous across any interface. Because the surface viscous stress tensor undergoes a discontinuous jump equal to $\sigma_{\rho\rho}=2\eta_2[dv_2/dr(r=a)]$ (assuming the surface viscous stress to be negligible inside a cavity), there must be a compensating discontinuity in the surface tension [15]. Integrating Eq. (10a) from $r=0$ to infinity, we obtain

$$\gamma_w=\gamma_0+\eta_3\int_0^\infty dr\frac{\partial}{\partial n}v_r(r,0)-2\eta_2\dot{a}/a. \quad (11)$$

This constitutes a self-consistency condition for the collapse rate of a cavity. The normal derivative of the flow velocity in Eq. (11)—the shear rate—can be calculated from Eq. (9):

$$\frac{\partial}{\partial n} v_r(r,0) = \frac{4}{\pi} \dot{a} a \frac{d}{dr}\left(\frac{K(a^2/r^2)}{r}\right), \tag{12}$$

with $K(m)$ the complete elliptical integral of the first kind. Using Eq. (12) in Eq. (11) leads to a logarithmic divergence at $r=a$ due to the singularity in the flow field. If we use the length scale δ introduced below Eq. (7) as a short-distance cutoff, we obtain a simple result:

$$\frac{da}{dt} \cong \frac{\Delta\Pi a(t)}{2[\eta_2 + \pi^{-1}\ln(4a(t)/\delta)\eta_3 a(t)]}. \tag{13}$$

The precise value of the cutoff is not important because Eq. (13) depends only weakly on δ.

(a) Surface viscous regime. Surface viscous losses dominate for cavity radii $a(t)$ small compared to the crossover length $\xi = \eta_2/\eta_3$. Equation (13) then reduces to

$$\frac{da}{dt} \cong -\Delta\Pi a(t)/2\eta_2. \tag{14}$$

The 2D cavity is thus predicted to shrink at a *constant rate* $\Delta\Pi/2\eta_2$, i.e., the radius should decrease exponentially in time:

$$a(t) = a_0 e^{-(\Delta\Pi/2\eta_2)t}. \tag{15}$$

The characteristic cavity lifetime $\tau = 2\eta_2/\Delta\Pi$ is independent of the initial radius of the cavity. Note that the surface viscous regime is just the 2D analog of cavity collapse in a 3D viscous fluid.

(b) Bulk viscous regime. For cavity radii large compared to $\xi = \eta_2/\eta_3$, viscous dissipation due to subphase flow dominates, in which case Eq. (13) reduces to

$$\frac{da}{dt} \propto -\frac{\Delta\Pi}{\ln(4a/\delta)\eta_3}. \tag{16}$$

The cavity now collapses at a nearly constant *velocity* $\Delta\Pi/\eta_3$, so the cavity lifetime $\tau(a)$ should be proportional to the initial radius and $a(t) \propto [\tau(a) - t]$. Once the cavity radius has dropped below ξ, collapse should once again take place at a constant rate as discussed above.

2. Isotropic 2D solids

The collapse dynamics of cavities in solids is controlled by the transport of vacancies and/or interstitials. We saw that the pressure at the cavity surface is less than that at the exterior boundary by an amount $\Delta\Pi$ that is fixed by thermodynamic considerations.

For every interstitial that diffuses from the exterior surface to the cavity surface, the free energy of the system is lowered by an amount $\Delta\Pi A_0$ with A_0 the area per particle (the same holds for the inverse process of vacancies produced at the cavity surface and transported to the exterior surface). Let the equilibrium area concentrations of interstitials and vacancies be, respectively, n^+ and n^- (with the product $n^+ n^-$ determined by the condition of detailed balance between vacancy and/or interstitial creation and recombination). The radial volume current density $J(r)$ moving outward from the cavity is equal to $n^+ v^+ - n^- v^-$ with $v^\pm$ the radial drift velocities of interstitials (vacancies). The force on an individual vacancy and/or interstitial is equal to the pressure gradient times the volume per particle, so the drift velocities are

$$\vec{v}^{\pm} = \pm \mu^{\pm} A_0 \vec{\nabla}\Pi \tag{17}$$

with $\mu^\pm$ the mobility of an interstitial or vacancy. For a 2D isotropic solid, the pressure profile obeys the Laplace law $\Delta\Pi = 0$, so a radial pressure profile can have only a logarithmic dependence on distance r. If L is the system size, then

$$\Pi(r) = -\Delta\Pi \frac{\ln(r/L)}{\ln(a/L)} \tag{18}$$

up to a constant. The resulting volume current density is

$$J(r) = -\frac{(n^+\mu^+ + n^-\mu^-)\Delta\Pi}{\ln(L/a)}\left(\frac{1}{r}\right). \tag{19}$$

Equating the volume current $I = 2\pi a J(a)$ with the reduction per unit time of cavity area $d/dt\ (\pi a^2)$ gives

$$\frac{d(\pi a^2)}{dt} = -2\pi \frac{(n^+\mu^+ + n^-\mu^-)\Delta\Pi}{\ln(L/a)}. \tag{20}$$

Equation (20) leads to the prediction that the cavity radius should decrease with time as $a(t) \propto [\tau(a) - t]^{1/2}$, with a cavity lifetime $\tau(a)$ that is proportional to the square of the initial radius.

C. Explosive cavitation

In Sec. II, LM microcavities generated at higher laser intensities were produced in an explosive way by the bursting of bubbles. The physics of thin-film rupture has already been extensively explored both for soap films [16] and for the bursting of macroscopic bubbles at the air-water interface [17]. Soap film bursts by the very rapid growth of a circular hole, which is bordered by a toroidal-shaped rim that contains part of the material that originally occupied the hole. The rim is preceded by a shock front (called the *aureole*) and it travels in a radial outward direction at a constant speed. Culik's relation [18] predicts that this speed should equal

$$V = \sqrt{\frac{2\gamma}{\rho h}}. \tag{21}$$

This relation is obtained by equating the total force exerted by the surface tension 2γ on the rim with the rate of change of the momentum (h is the film thickness and ρ is the density of the fluid). An important aspect of Eq. (21) is that, according to the law of momentum conservation, only *half* of the work done by the surface tension is transformed into kinetic energy. The remaining half must be dissipated in some manner [19], such as the production of jets of small droplets. Measured speeds of thicker films [16] agree well with Eq. (21). For thin films (e.g., a Newton black film with thickness

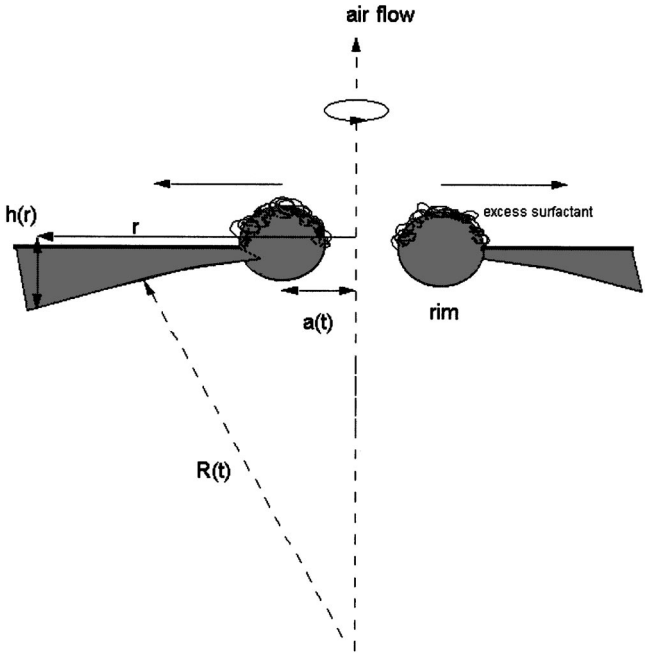

FIG. 10. Wormhole connecting the interior of a gas bubble just below a LM with the outside air. The hole, with diameter $a(t)$, is surrounded by a rim that travels in the radial outward direction under the action of the surface tension. The rim contains excess water and surfactant material that originally occupied the hole. The bubble diameter $R(t)$ diminishes because of air outflow.

of 100 nm or less), the rim exhibits a scalloped shape [20] and the speed is somewhat less than expected from Eq. (21). The Culik velocity is about 10 m/s for a film with thickness $h=100$ nm so a 1 μm size hole is formed in only 10^{-7} s. Somewhat closer to the problem of cavitation by bubble bursting in LM's is the problem of air bubbles bursting at an air-water surface. A growing rim is again observed in this case, moving with velocities of order m/s. In addition, a spray of tiny droplets is seen [17] (connected perhaps to a Rayleigh instability of the rim). Energy dissipation by bursting bubbles is in fact so intense that it may cause cell death for cells residing at an air-water interface [21].

Assume a surfactant-free, micrometer-sized, gas-filled spherical bubble of radius R touching a LM (from below). The film separating the bubble from the air is asymmetric: surfactants only cover the top of the film. Assume also that the air-water interface is flat (the buoyancy force on the bubble is too weak to deform the interface) and that the film thickness $h(0)$ at the point where the bubble touches the LM is microscopic, i.e., comparable to the size of a surfactant molecule. As a function of the distance r, the thickness profile $h(r)$ of the water layer is then given by

$$h(r)\cong\frac{1}{2}\frac{r^2}{R}. \tag{22}$$

At $t=0$ (the moment the bubble bursts) we introduce a small hole at $r=0$, the thinnest part of the film, in the form of a wormhole that connects the gas bubble interior with the outside air (see Fig. 10).

Three processes must start.

(1) The hole is subject to a force per unit length equal to the *sum* of the tensions of the top and bottom part of the film. This causes the hole to widen, with formation of a rim (see Fig. 10).

(2) The boundary line separating surfactant-covered and surfactant-free surface is subject to a force per unit length equal to the *difference* in surface tensions. This causes the surfactants to invade the hole.

(3) Gas escapes from the bubble due to gas flow through the hole, driven by the Laplace pressure of the bubble interior. This causes the bubble radius $R(t)$ to reduce in time.

We start with the first process. The hole rim is subject to a surface tension γ_0 from the LM on the top part of the film and to the bare surface tension of water γ_w from the bottom part of the film. The total force per unit length f on the hole rim equals

$$f=(2\gamma_w-\Pi). \tag{23}$$

Integrating Eq. (22), we find for the mass $M(a)$ per unit length of rim

$$M(a)\cong\frac{1}{8}\rho\frac{a^3}{R} \tag{24}$$

with $a(t)$ the time-dependent radius of the hole. The momentum per unit length $P(t)$ stored in the moving rim equals $M(a)(da/dt)$. Equating $dP(t)/dt$ to the force per unit length f gives

$$\frac{d}{dt}\left(\frac{\rho a^3}{8R}(da/dt)\right)=(2\gamma_w-\Pi). \tag{25}$$

If the radius R of the bubble is kept fixed to be R_0, then the solution of Eq. (25) is [22]

$$a(t)=\left[\frac{16R_0(2\gamma_w-\Pi)}{\rho}\right]^{1/4}t^{1/2}\quad(\text{fixed } R). \tag{26}$$

Unlike the case of a bursting soap film, the velocity of the rim is *not* constant: the speed drops inversely with the square root of time, because the film thickness increases as the hole widens.

Once the hole radius is comparable to the bubble thickness R, the bubble has effectively fused with the surface. The bubble/surface fusion time $\tau(R)$ can thus be estimated by the condition that $a(\tau)$ must be of order R:

$$\tau(R)\cong\left[\frac{\rho}{(2\gamma_w-\Pi)}\right]^{1/2}R^{3/2}\quad(\text{fixed } R). \tag{27}$$

For a 10 μm bubble, the fusion time is of the order of 10^{-5} s. This is much less than the cavity relaxation time $2\eta_2/\Delta\Pi$ obtained above, which means that the second process, surfactant invasion, can be neglected for all intents and purposes.

Just as for the soap film case, only part of the surface energy can be transformed into rim kinetic energy. The total work done per unit length of rim by the applied force f at a time T,

$$\int_0^T dt\, f\left(\frac{da}{dt}\right) = fa(T) = 2M(a)\left(\frac{da(T)}{dT}\right)^2, \tag{28}$$

equals *four* times the kinetic energy, not just twice as in the case of flat films. This means that now not 1/2 but 3/4 of the surface energy must be dissipated in the rim. Because the surfactant material that originally occupied the area πa^2 on the top half of the film is restricted to the rim, which has a surface area that is less by a factor $(a/R)^{1/2}$, we expect that the surfactant material of the rim is in ''collapsed'' form, which may absorb part of the excess kinetic energy. An alternative possibility is the formation of surfactant micelles.

We assumed so far that the radius of the bubble was constant during the bursting, but the bubble will reduce in size as it vents gas through the aperture. This process has been carefully examined for bursting vesicles [23]. The velocity $v(a)$ of the air emerging through a hole is related to $R(t)$ by mass conservation:

$$v(a) \approx -\left(\frac{R}{a}\right)^2 \frac{dR}{dt}. \tag{29}$$

Balancing the viscous dissipation by the air flow with the work done per second by the surface tension of the gas bubble gives

$$\frac{dR}{dt} \propto -\frac{\gamma_w}{\eta_a}\frac{a^3}{R^3} \tag{30}$$

with η_a the viscosity of air. To compute the corrected fusion time, Eqs. (25) and (30) must be solved simultaneously:

$$R(t) = \left(R(0)^4 - C_1 \frac{\gamma_w}{\eta_a}\int_0^t a^3(t')dt'\right)^{1/4} \tag{31}$$

with C_1 a numerical factor. If the factor $(\gamma_w/\eta_a)\int_0^t a^3(t')dt'$ remains small compared to $R(0)^4$ up to the fusion point where $a(t)$ is comparable to $R(0)$, then bubble deflation plays no role and Eq. (17) remains valid. The ''fixed R'' condition is

$$\frac{\gamma_w}{\eta_a}\int_0^{\tau(R)} a^3(t')dt' < R^4. \tag{32}$$

Using Eqs. (26) and (27), we find that the fixed R regime holds only for bubbles whose radius obeys the inequality

$$R < \left(\frac{f}{\rho}\right)\left(\frac{\eta_a}{\gamma_w}\right)^2. \tag{33}$$

If the inequality Eq. (33) does not hold, then the bubble must at least partially deflate during cavity formation, leading to a reduction of the eventual cavity size. The fusion time is determined by equating $(\gamma_w/\eta_a)\int_0^{\tau(R)} a^3(t')dt'$ with $R(0)^4$:

$$\tau(R) \propto R^{13/10}\left(\frac{\eta_a}{\gamma_w}\right)^{2/5}\left(\frac{\rho}{f}\right)^{3/10}. \tag{34}$$

IV. CONCLUSIONS

In this section we reexamine the experiments of Sec. II in the light of the theoretical description of cavity initiation and collapse presented in Sec. III.

A. Cavity collapse in a LC phase

In Sec. II we saw that cavities created by low heating in the LC phase of 10,12-pentacosadiyonic acid with $\Pi = 25$ mN/m and $T = 18\,^\circ$C collapsed with a characteristic time of the order of seconds, though not all cavities closed. The time-dependent cavity radius could be fitted as a power law $a \propto (t_c - t)^\beta$ with exponents β approximately in the range 0.2 ± 0.1. This form for the time dependence would be quite inconsistent with Eq. (15) for the collapse of cavities in fluid LM's. However, for cavity collapse in the solid phase vacancy and/or interstitial diffusion the cavity radius should decrease as $a(t) \propto (t_c - t)^{1/2}$, reasonably close to the measured time-dependent radius (although an exponent $\beta = 1/2$ would lie outside the experimental error bar). The observation of extensive dendritic growth would seem to provide support for this interpretation. It is likely that a refinement of the model taking into account the fractal growth using nonradial symmetric solutions of the Laplace equation for the surface pressure will result in a reduced collapse exponent closer to the experiment. Little is known about the concentrations of vacancies and/or interstitials in LM's and their mobilities, so it is not possible to quantitatively compare calculated and measured cavity lifetimes.

B. Cavity collapse in a LE phase

In Sec. II, we found that cavities in the LE phase of pentadecanoic acid ($A = 76.5$ Å^2, $T = 22\,^\circ$C) collapsed in less than a second. The time dependence of the cavity radius could be fitted as $a \propto t^\beta$ with β in the range -0.8 ± 0.1. If the rheology of the LE phase is that of an isotropic incompressible 2D liquid, then Eq. (13) should hold. To apply Eq. (13), we first need to estimate the crossover length $\xi = \eta_2/\eta_3$ and compare it with a typical cavity size. Accurate measurements of η_2 in the LE phase do not appear to be available but, if we estimate the surface viscosity [24] by treating the LE phase as a layer of thickness 30 Å having a typical alkane viscosity of 1–10 P, we obtain a range of 10^{-6}–10^{-7} g/s. The crossover length is then of order 1 μm or less, so we should assume the bulk viscous regime [Eq. (15)] for cavity collapse in the LE phase.

The prediction is then that the cavity should collapse with a constant velocity $\Delta\Pi/2\eta_3$, which is of the order of 10^3 cm/s. This is much too fast compared with observed collapse velocities, which are at most 10 μm/s, so we have to conclude that surfactant transport in the LE phase cannot be treated as hydrodynamic flow of a 2D incompressible fluid coupled to a 3D subphase. This should perhaps not be surprising, since the LE phase is indeed quite compressible

compared to the LC phase. A consequence of this is that a gradient in the area density is expected to develop around the cavity, which would lead to a drop in the effective pressure difference across the cavity surface and a slowdown of the kinetics at later times. If we ignore coupling to the subphase and treat transport in the LE phase as that of a dense 2D solution with a collective diffusion constant $D_c = \mu\, d\Pi/dc$ (μ is the surfactant mobility and c the surfactant area concentration), we obtain a much more reasonable cavity collapse time $\tau(a) \propto (a^2/D_c)$ of the order of seconds (a is of order 10 μm and D_c is in the range 10^{-6} cm^2/s.) However, the associated time dependence of the radius, again proportional to $[\tau(a)-t]^{1/2}$, would not agree with the experimental results, so the cavity collapse kinetics of the LE phase remains to be explained.

It should be noted that for the fluid LC phases surface viscosities are much larger. For octadecanol for instance, it is of order g/s [25,26] while for eicosanoic acid it is of order 10^{-2}–10^{-3} g/s [9]. For LC phases in the fluid state (such as hexatics), the surface viscous regime would thus be appropriate. The predicted collapse time $\Delta\Pi/2\eta_2$ is then in excess of 10 s, which is in quite reasonable agreement with observed cavity collapse times in the LC phase, and the assumption of incompressibility is quite reasonable for LC phases. However, we did not encounter so far in any of our experiments on the LC phase the predicted ''fixed-rate'' collapse kinetics associated with cavity collapse in the surface viscous regime of Eq. (13).

C. Explosive cavitation

The last two experiments described in Sec. III concerned explosive cavitation by bubble bursting. For an octadecanol LM in the LC phase ($T = 25\,^\circ$C, $\pi \approx 16.5$ mN/m), bubble bursting took place at submillisecond time scales and was accompanied by capillary wave emission. After the rupture event, either star-shaped holes were observed with concave surface sections (small bubbles) or convex hexagonal holes (large bubbles) containing a virtual topological defect. In the latter case, small explosion fragments were observed to diffuse around in the cavity.

The calculated cavity formation time, Eq. (27), is in the submillisecond range, which is consistent with our observations. The fact that many small fragments of surfactant material are produced during cavitation is consistent with observation reported by studies of the bursting of macroscopic bubbles, as discussed in Sec. III. It indicates that the surfactant-rich rim broke up during the formation of the cavity.

Comparison between theory and experiment, however, produces a number of discrepancies. It follows from Eq. (23) that the ratio of the maximum hole diameter $a(\tau)$ and the initial bubble radius equals

$$\frac{a(\tau)}{R} \approx \left(\frac{\eta_a}{\gamma_w}\right)^{1/5} \left(\frac{f}{\rho R}\right)^{1/10}. \tag{35}$$

For instance, for a bubble with an initial radius of 10 μm, the right hand side is of order 0.1. The maximum size of the surfactant-free area produced by bubble bursting is thus predicted to be of the order of 0.1 of the bubble radius. For the bursting event shown in Fig. 5, the final cavity actually has a radius that is *larger* than that of the bubble. Next, we noted that large bubbles produce convex hexagonal shapes and small bubbles concave star shapes. The obvious interpretation would be that the kinetics of cavitation must be faster for smaller bubbles. However, according to Eq. (26) the cavity growth kinetics is actually predicted to be faster for large bubbles.

The most puzzling observation, however, is the fact that none of the cavities produced by the bubble bursting method closed. It would seem that this provides evidence that the LC phase is solid. However, compare the case of cavities in 10,12-pentacosadiynoic acid at $\Pi = 25$ mN/m, $T = 18\,^\circ$C produced by lower intensity ir heating, as shown in Fig. 1, with that of Fig. 8, where the cavities were produced by bubble bursting. The same material was used and the same thermodynamic conditions prevailed. Evidently, the structural properties of the cavities in the two cases are not the same: structure and lifetime of a LM cavity depend on the method of cavitation. One interpretation is that during explosive cavitation the positional and orientational order are perturbed to a high degree. In particular, production of disclination pairs may have taken place in that case. The fact that explosive cavitation may produce topological defects is supported by the observations on the tilt degree of freedom in Fig. 6. The fact that explosion cavities initially tend to be star shaped (see Fig. 8) could be interpreted as providing evidence for disclination-type defects and/or grain-boundary lines. The presence of such defects could retard the closure kinetics since the filling in of the cavity might generate increasing elastic stress. Similarly, filling in the cavity of Fig. 6 must produce an increase in the free energy of the tilt degree of freedom when our virtual topological defect becomes an actual topological defect, with a large elastic distortion in the defect core.

ACKNOWLEDGMENTS

We would like to thank H. Möhwald for generous support and stimulating discussions, C. Knobler for reading the manuscript, and F. Brochard and S. Putterman for discussions on, respectively, the bursting of bubbles and cavitation. This work was supported by the Deutsche Forschungsgemeinschaft (DFG) through Grant Nos. Fi 548/2-1 and Fi 548/3-1.

[1] Lord Rayleigh, Philos. Mag. **34**, 94 (1917).
[2] C. Rottman and M. Wortis, Phys. Rep. **103**, 59 (1984).
[3] See, for instance, P. Chaikin and T. Lubensky, *Principles of Condensed Matter Physics* (Cambridge University Press, Cambridge, England, 1995), Chap. 9.5.
[4] R. M. Kenn, C. Böhm, A. M. Bibo, I. R. Peterson, and H. Möhwald, J. Phys. Chem. **95**, 2092 (1991).
[5] B. Lin, M. C. Shih, T. M. Bohanon, G. E. Ice, and P. Dutta,

Phys. Rev. Lett. **65**, 191 (1990).
[6] M. C. Shih, T. M. Bohanon, J. M. Mikrut, P. Zschack, and P. Dutta, Phys. Rev. A **45**, 5734 (1992).
[7] E. B. Sirota, Langmuir **13**, 3849 (1997).
[8] C. Zakri, A. Renault, J. P. Rieu, M. Vallade, B. Berge, J. F. Legrand, G. Vignault, and G. Grubel, Phys. Rev. B **55**, 14 163 (1997).
[9] M. L. Kurnaz and D. K. Schwartz, Phys. Rev. E **56**, 3378 (1997).
[10] S. Wurlitzer, C. Lautz, M. Liley, C. Duschl, and Th. M. Fischer, J. Phys. Chem. B **105**, 182 (2001).
[11] W. Rybczynski, Bull. Int. Acad. Sci. Cracovie Ser. A **1**, 40 (1911); J. S. Hadarmard, C. R. Hebd. Seances Acad. Sci. **152**, 1735 (1911).
[12] J. Rudnick and K. K. Loh, Phys. Rev. E **60**, 3045 (1999); D. K. Schwartz, M. W. Tsao, and C. M. Knobler, J. Chem. Phys. **101**, 8258 (1994).
[13] The line tension of the cavity boundary also performs work but for LM's this contribution is negligible for micrometer-sized cavities.
[14] R. de Koker and H. M. McConnell, J. Phys. Chem. B **102**, 6927 (1998).
[15] For a discussion of the 3D version of this equation, see L. D. Landau and E. M. Lifshitz, *Fluid Mechanics* (Pergamon, Oxford, 1981), Chap. 60.
[16] W. Mc Entee and K. Mysels, J. Phys. Chem. **73**, 3018 (1969).
[17] D. E. Spiel, J. Geophys. Res., [Space Phys.] **103**, 24 907 (1998), and references therein.
[18] F. E. Culik, J. Appl. Phys. **31**, 1128 (1960).
[19] For a discussion, see P.-G. de Gennes, Faraday Discuss. **104**, 1 (1996).
[20] L. Evers, S. Shulepov, and G. Frens, Faraday Discuss. **104**, 335 (1996).
[21] R. S. Cherry and C. T. Hulle, Biotechnol. Prog. **1**, 8 (1992).
[22] Equation (26) overestimates the rim speed during early stages of the hole formation. In a frame that moves with a velocity da/dt, the rim is stationary while the film is injected into the rim with a velocity da/dt. One obtains a limiting velocity f/η_3 from this dissipation mechanism that is of order 10 m/s. Equation (26) only applies for times t such that da/dt is less than f/η_3.
[23] O. Sandre, L. Moreaux, and F. Brochard-Wyart, Proc. Natl. Acad. Sci. U.S.A. **96**, 10 591 (1999).
[24] J. F. Klingler and H. M. McConnell, J. Phys. Chem. **97**, 6096 (1993).
[25] H. Hühnerfuss, J. Colloid Interface Sci. **107**, 84 (1985).
[26] H. Hühnerfuss, J. Colloid Interface Sci. **120**, 281 (1987).